





Article

S-Adenosyl-L-Methionine and Cu(II) Impact Green Plant Regeneration Efficiency

Renata Orłowska ¹, Jacek Zebrowski ², Janusz Zimny ¹, Piotr Androsiuk ³ and Piotr Tomasz Bednarek ^{1,*}¹ Plant Breeding and Acclimatization Institute—National Research Institute, Radzików, 05-870 Błonie, Poland² Institute of Biology and Biotechnology, University of Rzeszow, Pigoń 1, 35-310 Rzeszow, Poland³ Department of Plant Physiology, Genetics and Biotechnology, Faculty of Biology and Biotechnology, University of Warmia and Mazury in Olsztyn, 10-719 Olsztyn, Poland

* Correspondence: p.bednarek@ihar.edu.pl

Abstract: The biological improvement of triticale, a cereal of increasing importance in agriculture, may be accelerated via the production of doubled haploid lines using in vitro culture. Among the relevant factors affecting the culture efficiency are Cu(II) or Ag(I) acting, e.g., as cofactors of enzymes. The copper ions are known to positively affect green plant regeneration efficiency. However, the biochemical basis, mainly its role in the generation of in vitro-induced genetic and epigenetic variation and green plant regeneration efficiency, is not well understood. Here, we employed structural equation modeling to evaluate the relationship between de novo DNA methylation affecting the asymmetric context of CHH sequences, the methylation-sensitive Amplified Fragment Length Polymorphism related sequence variation, and the concentration of Cu(II) and Ag(I) ions in induction media, as well as their effect on S-adenosyl-L-methionine perturbations, observed using FTIR spectroscopy, and the green plant regeneration efficiency. Our results allowed the construction of a theory-based model reflecting the biological phenomena associated with green plant regeneration efficiency. Furthermore, it is shown that Cu(II) ions in induction media affect plant regeneration, and by manipulating their concentration, the regeneration efficiency can be altered. Additionally, S-adenosyl-L-methionine is involved in the efficiency of green plant regeneration through methylation of the asymmetric CHH sequence related to de novo methylation. This shows that the Yang cycle may impact the production of green regenerants.

Keywords: anther culture; copper; genetic variation; metAFLP; S-adenosyl-L-methionine; silver; triticale



Citation: Orłowska, R.; Zebrowski, J.; Zimny, J.; Androsiuk, P.; Bednarek, P.T. S-Adenosyl-L-Methionine and Cu(II) Impact Green Plant Regeneration Efficiency. *Cells* **2022**, *11*, 2700. <https://doi.org/10.3390/cells11172700>

Academic Editor: Suleyman Allakhverdiev

Received: 18 July 2022

Accepted: 25 August 2022

Published: 30 August 2022

Publisher's Note: MDPI stays neutral with regard to jurisdictional claims in published maps and institutional affiliations.



Copyright: © 2022 by the authors. Licensee MDPI, Basel, Switzerland. This article is an open access article distributed under the terms and conditions of the Creative Commons Attribution (CC BY) license (<https://creativecommons.org/licenses/by/4.0/>).

1. Introduction

Triticale is an allopolyploid plant that was generated artificially [1] and is reasonably simple for in vitro plant regeneration [2], resulting in doubled haploid (DH) lines that could be utilized for the evaluation of new varieties [3]. Chromosome elimination [4] or microspore embryogenesis (androgenesis) [5] are two methods that could be used to create DH plants. In order to take advantage of androgenesis, isolated microspore cultures [6] or anther cultures [7] are used. Green plant regeneration efficiency (GPRE) is constrained by tissue culture media or genotype in both situations [8]. Furthermore, poor spontaneous chromosome duplication [9,10], ineffective regeneration from androgenic structures [11], and the dominance of albino over green regenerants [12,13] are all factors that limit GPRE, with the latter being the most problematic.

From cytological examinations to genomic studies focused on the plastid and nuclear genes, research pertaining to the origin of albino plants have been conducted [14]. Recent investigation on albino plants has revealed a considerable genotypic influence on molecular variations related to chloroplast differentiation in the formation of green and albino regenerants through isolated microspore cultures [15]. According to Sakamoto [16] and Clément [17], the production of amyloplasts from proplastids is necessary for the

acquisition of green regenerants. The lack of proplastids prevents the nascent regenerants from carrying out photosynthesis and, thus, does not allow them to function outside the *in vitro* culture [18–20]. From current research on albinism, which takes into account both gene level and studies on structural changes in plastids during androgenesis, it may be deduced that crosstalk between plastid and nuclear genomes is crucial for the appropriate development and function of the chloroplasts and the cell. Through anterograde and retrograde signaling between the cell nucleus and plastid genomes, both genomes are coordinated. However, there are not many interdisciplinary studies relating different GPRE characteristics (such as genetic, epigenetic, metabolomic, and transcriptomic) in cereals.

Ion components constituting the induction media (IM) have the potential to have a significant impact on GPRE [21]. The copper, zinc, and silver ions were notable among the IM constituents. When employed at the proper concentrations, each of these ions had a favorable impact on GPRE [22–25]. The biochemistry of GPRE and its relationship to *de novo* methylation, sequence variation, and metal ion concentrations in the IM are, however, poorly understood.

Copper ions (Cu(II)) are elements of proteins such as plastocyanin (act as a cofactor) [26] and cytochrome *c* oxidase [27] involved in electron transport in chloroplast and mitochondria, respectively, and copper/zinc superoxide dismutase (Cu/Zn-SOD) found in the cytosol and chloroplast of plants [28]. By changing the concentrations of Cu(II), it is possible to change the photochemical activity of cells [29,30] or the way enzymes work [31]. Copper ion deficit due to poor ATP generation caused by cytochrome *c* oxidase malfunction may have an impact on S-adenosyl-L-methionine (SAM) production [32–34]. Involved in cellular methylation processes like cytosine methylation, SAM is produced in the Yang cycle [35,36]. As suggested by studies on barley [37], SAM may be essential for controlling gene expression [38,39] in order to linking varying parts of GPRE. However, it is not clear if SAM is also involved in GPRE in triticale or if the various components that contribute to the phenomena interact similarly in different species.

If a specially created biological system based on a (epi)genetically uniform progeny of a DH plant is employed as a source of tissue explants for the acquisition of regenerants, research on the genetic and epigenetic components of GPRE might be conducted. When such a system is used, the so-called pre-existing variation [40,41] that may affect the overall variance assessed between regenerants is practically eliminated [42].

Additionally, a molecular marker system that can detect and measure (epi)genetic variation is required. The preferred techniques are Methylation-Sensitive Amplified Polymorphism (MSAP) [43] and methylation-sensitive Amplified Fragment Length Polymorphism (metAFLP) [44]. To quantify sequence variation (SV), DNA demethylation (DMV), and *de novo* methylation (DNMV) simultaneously, only the metAFLP is available. As shown in some cereals [45,46], it is likewise capable of measuring symmetric (CG, CHG) and asymmetric (CHH) (H is A, C, or T) DNA sequence contexts, where cytosine can be methylated. When only methylation changes are considered, then MSAP could be utilized [44].

A quick, label-free, non-destructive method for determining the metabolome profile of biological samples is infrared spectroscopy, which enables the assessment of a plant's physiological state, as well as how well it responds to various environmental factors [47–52]. Typical plant tissue spectra exhibit several bands caused by the superimposition of a variety of chemical components. Numerous statistical and/or chemometric techniques have been used to extract more detailed information from the spectra, including supervised and unsupervised techniques [53–59]. Regression analysis and calibration standards are combined in this technique to enable the measurement of specific elements in the material under study [60–62]. As shown in experiments on barley by Bednarek [44], it might also be used to quantify a variety of products of metabolic cycles of pathways including SAM.

It is difficult to identify the most critical predictors of any phenomena without sufficient statistical tools and numerous data derived through many methods. This is especially the case when testing a hypothesis describing relationships between varying aspects of a phenomenon. Recently, moderation [43], mediation [46], and structural equation modeling

(SEM) statistical methods derived from psychological studies were applied to studies of anther tissue cultures in barley [44]. Furthermore, combining molecular and biochemical (i.e., metabolomic) information and applying moderation, mediation, or SEM to the situation may result in theory-based models that combine various aspects of GPPE into a single framework.

We hypothesized that producing triticales DH regenerants via anther cultures following varying conditions (including the IM ingredients concentrations and time of cultures) from a single uniform plant that is the progeny of a doubled haploid would distinctly alter DNA methylation, disrupt biochemical cycles (i.e., Krebs, Yang), and adjust the metabolome (like SAM) in a way that would have an impact on GPPE. The datasets can be placed in a statistical context to demonstrate their relationships and provide an explanation for GPPE based on biological processes.

The purpose of the study was to evaluate the interactions between de novo DNA methylation affecting the asymmetric sequence context CHH, respective sequence variation assessed with the metAFLP technique [45], Cu(II) and Ag(I) ion concentrations in the IM, and their effects on SAM disturbances revealed via Fourier Transfer Infrared (FTIR) spectroscopy affecting GPPE, using structural equation modeling.

2. Materials and Methods

The studies were performed on donor plants and regenerants of hexaploid triticales cultivar T28/2 obtained from a cross between cv. Presto \times cv. Mungis. The seeds were provided courtesy of Sylwia Oleszczuk (Plant Breeding and Acclimatization Institute-National Research Institute, Radzików, Poland). Donor plants and regenerants were derived as described elsewhere [63]. Donor plants were the generative progeny of regenerants derived by androgenesis. In addition, donor plants were the source of explants (anthers) for obtaining regenerants. Supplementing induction media with Cu(II) and silver (Ag(I)) ions were tested, and the effect of anther incubation time on induction media was studied. Eight (A-H) different triticales regeneration conditions were tested in the experiment.

The metAFLP technique was used to generate the molecular data [45,64]. The quantification of in vitro-induced variation and its components, SV, DN MV, and DMV, including symmetric (CG and CHG) and asymmetric (CHH) sequence contexts, was performed as described earlier [45].

For the infrared spectroscopy, we used plant material obtained earlier [46]. It consisted of 37 regenerants encompassing eight (A-H) different in vitro conditions. In brief, the infrared spectra were collected from lyophilized and homogenized (ball milled, MM 400, Retsch, Haan, Germany) plant tissues by means of the iZ10 spectrometer (Thermo Fisher Scientific, Waltham, MA, USA) in the Attenuated Total Reflectance (ATR) mode equipped with a deuterated triglycine sulfate (DTGS). The sixty-four scans captured at the 4 cm^{-1} resolution were averaged, ATR and baseline corrected using OMNIC (v.9.0, Thermo Fisher Scientific, Waltham, MA, USA) software. Following that, the data were Savitzky-Golay smoothed (to reduce high-frequency noise in a signal) and normalized to the unit area ($1800\text{--}900\text{ cm}^{-1}$) using the hyperSpec package [65] on the R platform [66]. Based on the spectra, absorbances were summarized within 10 cm^{-1} wide intervals across the spectra range from $600\text{ to }3800\text{ cm}^{-1}$ using the hyperSpec package. Furthermore, the SAM reference sample (#A4377, Sigma-Aldrich, St. Louis, MO, USA) was analyzed using the same equipment and procedure as the one mentioned above.

The SEM was performed using AmosTM 20 [67] computer software under IBM SPSS[®] [68]. The maximum likelihood (ML) estimation with the Levenberg–Marquardt iteration method [69–71] was used to optimize the parameters of proposed models.

3. Results

Pachota [63] previously described morphologically uniform donor plants and their regenerants in terms of plant development, leaf shape, color, width, tillering mechanism, and spike number. Orłowska [46] published the quantitative metAFLP features relating to

DNA de novo methylation and sequence variation in the asymmetric sequence contexts (CHH). The same is true for the estimation of GPRE [45]. So, Table 1 only shows the GPRE, metAFLP quantitative features and in vitro tissue culture conditions for simplicity.

Table 1. Tissue culture conditions used for plant regeneration by trials A-H, metAFLP quantitative characteristics, the IR spectra region and green plant regeneration efficiency.

Trial	In vitro Anther Culture Conditions *			metAFLP Quantitative Characteristics (%) *		IR Spectra Region, cm ⁻¹					GPRE *	
	Cu	Ag	T	CHH_SV	CHH_DNMV	1300–1310	1390–1410	1470–1490	1570–1630	1770–1780		1470 ... 1630
A	0.1	10	42	8.66	0.37	0.185803	1.26907	0.42455	2.98543	0.002389	3.40998	0.87
	0.1	10	42	8.66	0.37	0.183574	1.13292	0.43707	3.24874	0.001217	3.68581	0.87
	0.1	10	42	8.52	0.36	0.191639	1.04731	0.53558	3.71659	0.001245	4.25217	0.87
B	0.1	60	49	8.64	0.37	0.178196	1.2209	0.38154	2.85966	0.001426	3.24120	1.52
	0.1	60	49	8.64	0.37	0.254396	1.74913	0.48147	3.51083	0.001349	3.99229	1.52
	0.1	60	49	8.79	0.37	0.227685	1.43375	0.47772	3.48294	0.000922	3.96066	1.52
	0.1	60	49	8.79	0.37	0.175904	1.25097	0.37122	2.89457	0.000428	3.26579	1.52
	0.1	60	49	8.79	0.56	0.202656	0.96207	0.48410	3.35658	0.00006	3.84068	1.52
C	5	60	42	8.76	0.75	0.225474	1.74601	0.48503	3.83905	0.001269	4.32409	0.71
	5	60	42	8.79	0.56	0.190203	0.95596	0.48507	3.77714	0.002415	4.26221	0.71
	5	60	42	8.64	0.55	0.186824	1.69150	0.41648	2.93397	0.003896	3.35044	0.71
D	5	0	49	8.64	0.55	0.219423	1.09671	0.50444	3.83734	0.00393	4.34178	2.38
	5	0	49	8.64	0.55	0.21104	1.07641	0.51469	3.70682	0.002942	4.22150	2.38
	5	0	49	8.76	0.75	0.169463	0.85519	0.48458	3.48811	0.001751	3.97269	2.38
	5	0	49	8.76	0.75	0.233781	1.04895	0.58042	4.02282	0.002706	4.60325	2.38
	5	0	49	8.76	0.75	0.215361	1.54017	0.51606	3.50145	0.002085	4.01752	2.38
	5	0	49	8.76	0.75	0.183114	1.07270	0.49534	3.49364	0.002132	3.98898	2.38
	5	0	49	8.76	0.75	0.210347	1.47711	0.52601	3.73455	0.000688	4.26056	2.38
	5	0	49	8.76	0.75	0.245707	1.15563	0.57322	4.04161	0.000517	4.61482	2.38
	5	0	49	8.76	0.75	0.214937	1.80068	0.47137	3.71232	0.001001	4.18367	2.38
E	5	10	35	8.91	0.76	0.238564	1.38936	0.51576	4.03064	0.001575	4.54641	2.38
	5	10	35	8.63	0.73	0.250745	1.47001	0.55275	3.68871	0.000681	4.24147	1.17
	5	10	35	8.63	0.73	0.200508	1.00326	0.42343	3.09758	0.001475	3.52101	1.17
	5	10	35	8.48	0.72	0.211908	0.99925	0.45294	3.30125	0.002535	3.75418	1.17
	5	10	35	8.48	0.72	0.225066	1.02850	0.53925	3.54277	0.000399	4.08202	1.17
F	5	10	35	8.5	0.54	0.273647	1.55344	0.54718	3.63317	0.00004	4.18035	1.17
	10	10	49	8.48	0.54	0.182705	1.40998	0.38534	2.92596	0.000861	3.31130	3.79
	10	10	49	8.65	0.55	0.185444	1.32401	0.38477	2.95017	0.000606	3.33494	3.79
	10	10	49	8.65	0.55	0.188182	1.04185	0.43797	3.20739	0.000536	3.64536	3.79
	10	10	49	8.65	0.55	0.188182	1.04185	0.43797	3.20739	0.000536	3.64536	3.79
G	10	60	35	8.62	0.56	0.265116	1.81778	0.56006	3.96663	0.002101	4.52669	4.24
	10	60	35	8.49	0.55	0.252854	1.26877	0.58166	3.83262	0.002195	4.41428	4.24
	10	60	35	8.49	0.55	0.253788	1.05274	0.61500	4.03725	0.004113	4.65225	4.24
	10	60	35	8.65	0.55	0.251024	1.68097	0.48234	3.44185	0.00196	3.92419	4.24
H	10	0	42	8.49	0.55	0.221811	1.06542	0.53357	3.73425	0.000346	4.26782	6.06
	10	0	42	8.49	0.55	0.198332	0.97900	0.46960	3.39556	0.001703	3.86516	6.06
	10	0	42	8.65	0.55	0.188945	1.448	0.29188	2.36092	0.003409	2.65280	6.06
	10	0	42	8.65	0.55	0.197657	0.92487	0.46271	3.40941	0.001247	3.87212	6.06

* Data obtained previously as mentioned in the “Material and methods” section; the metAFLP quantitative characteristics concerning sequence variation (CHH_SV) and de novo DNA methylation (CHH_DNMV) between donor plant and its regenerants affect asymmetric CHH sequence contexts; GPRE—green plant regeneration efficiency (number of regenerants per 100 plated anthers on induction medium); IR—infra-red.

The infrared spectrum of the SAM compound used as a standard revealed the presence of broadband between 2700 and 3500 cm⁻¹ (insert in Figure 1). This absorbance region is attributed mainly to the O-H stretching from ribose and methionine, with only very small local absorbances at 3314 and 3172 cm⁻¹, possibly due to the N-H stretching of the amide groups. Additional small local peaks at 2982 and 2909 cm⁻¹ are probably derived from the C-H stretching vibrations. Unfortunately, this spectra range did not offer clear high or medium-intensity infrared signals and thus was not used in further analyses as a characteristic of SAM.

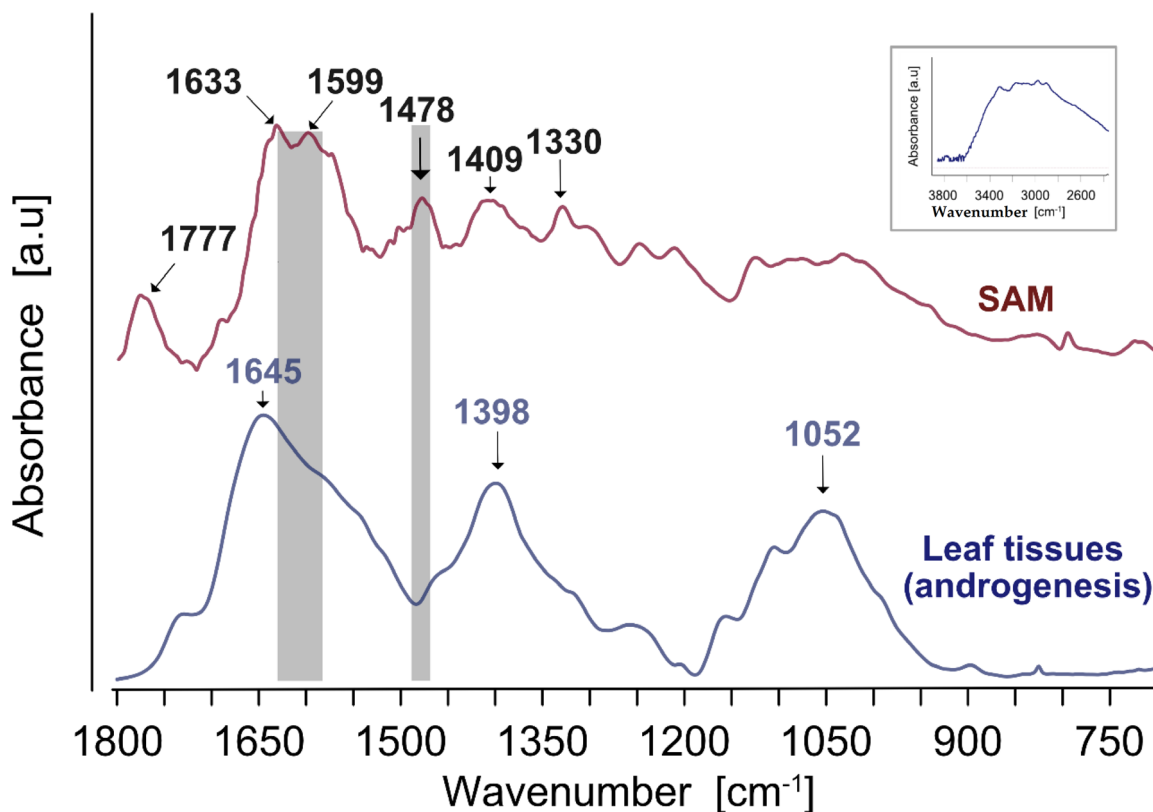


Figure 1. The infrared spectrum of S-adenosyl-L-methionine (upper) and the mean spectrum of leaf tissues (lower). The latter was averaged over all experimental treatments. The major bands are indicated with arrows. The fitted spectra regions in the structural equation modeling are shaded in grey. The inset presents the high-frequency spectral region of SAM.

The SAM infrared spectra in the region between 1800 and 600 cm^{-1} (Figure 1, upper) showed a band at 1777 cm^{-1} , which can be tentatively assigned to C=O stretching, and the double most pronounced peak at around 1600–1630 cm^{-1} . The latter may be associated with signals from methionine, namely due to C-C, C-N stretching, the NH_2 scissoring, and asymmetric stretch of COO^- [72,73] as well as from pyrimidine ring vibrations coupled with the NH_2 scissoring mode of adenosine [74,75]. Other medium bands at 1478 and 1409 cm^{-1} may be attributed to the C-N, C-C stretching, CH_3 deformation, and NH_2 bending, while the band at 1330 cm^{-1} is mainly due to the stretch of the C-N, C=N of an adenine ring, and twisting of CH_2 groups in methionine [76]. Additionally, relatively weaker peaks were distinguished at 1279, 1248, and 1074 cm^{-1} , possibly due to the C-C, C-N stretch, and rocking vibrations of NH_2 deformation [75]. Small absorbances at 821 and 726 cm^{-1} may be attributed to the 5-ring and 6-ring deformations, respectively [76]. Thus, only FTIR wavenumbers assigned to bands allocated to the SAM (around 1330, 1410, 1480, 1580–1630, and 1780 cm^{-1}) and present within 1300–1780 cm^{-1} were implemented in further analyses.

Averaged infrared spectra of leaf tissues (Figure 1 lower) showed the most pronounced broadband in the Amide I region, centered at 1645 cm^{-1} , possibly due to C-C, C=C, C-N stretching, and NH_2 deformation. Two complex bands in the fingerprint region were present at 1398 and 1052 cm^{-1} . The former could be assigned to vibration modes also attributed to SAM, while the latter was mainly from sugars and structural polysaccharides (the C-C, C-O, and C-C-O stretching) (polysaccharides [77]). The spectra of leaves showed relatively broadband with overlapping absorbances from various chemical compounds in the tissues. Not all FTIR bands detected for SAM were visualized on the leaf spectra. Still, they were implemented in the structural equation modeling to identify the regions reflecting SAM vibrations and fit the postulated model. Furthermore, the range of wavenumbers

corresponding to absorbances (summarized over 10 cm⁻¹ bands) characteristic of SAM was tested (the most relevant signals from SAM are shaded grey in Figure 1).

The postulated model assumed that prominent FTIR bands identified in the SAM spectrum affected de novo DNA methylation (SAM is the cell methylation agent) within different sequence contexts. DNA methylation is influenced by Cu(II) ions, leading to modified methylated cytosines followed by sequence variation. DNMT, SV, and Cu(II) influence GPRE. However, DNMT impacts epigenetic regulation, while Cu(II) affects biochemical pathways, influencing epigenetic mechanisms.

All FTIR bands assigned to SAM within the 1300–1780 cm⁻¹ range were tested to fit the postulated model (Table 2). They resulted in at least well-fitting models; however, only the 1590–1630 and 1470–1490 cm⁻¹ spectral regions and their combination (1470 . . . 1630 cm⁻¹) gave rise to nearly all significant paths. In contrast, the others failed to identify the significant path toward the DNA methylation variable or sequence variation and did not affect GPRE. Thus, the final SEM model was constructed using only the 1470 . . . 1630cm⁻¹ spectral region.

Table 2. The arrangement of SEM goodness-of-fit statistics implementing five FTIR spectra ranges related to SAM.

Fit Indices	FTIR Spectra Intervals (Wavenumbers, cm ⁻¹)					1580–1630; 1470–1490 = 1470 . . . 1630
	1300–1310	1390–1410	1470–1490	1580–1630	1770–1780	
χ^2	1.2544	3.7445	2.2677	0.0191	0.7437	0.1095
<i>p</i>	0.5341	0.1538	0.3218	0.99905	0.6892	0.9467
<i>df</i>	2	2	2	2	2	2
RMR	0.0006	0.0121	0.0007	0.0013	0.0000	0.0020
GFI	0.9865	0.9620	0.9762	0.9948	0.9919	0.9988
AGFI	0.8987	0.7149	0.8212	0.9984	0.9392	0.9909
PGFI	0.1315	0.1283	0.1302	0.1333	0.1323	0.1332
NFI	0.9819	0.9962	0.9688	0.9997	0.9891	0.9985
RFI	0.9094	0.7311	0.8439	0.9987	0.9954	0.9924
IFI	1.0111	0.9742	0.9962	1.0283	1.0190	1.0027
TLI	1.0629	0.8537	0.9786	1.1596	1.1081	1.1525
CFI	1	0.9707	0.9957	1	1	1
PNFI	0.1964	0.1892	0.1938	0.1944	0.1978	0.1997
PCFI	0.2	0.1941	0.1991	0.2	0.2	0.2
RMSEA	0	0.1557	0.0610	0	0	0
SRMR	0.0392	0.0478	0.0502	0.0045	0.0182	0.0112

The structural equation modeling analysis was based on 37 regenerants representing eight experimental trials (Table 3). A slight deviation from the normal distribution was observed based on skewness and kurtosis values. However, all variables were quantitative and fulfilled the conditions of the Lindeberg–Lévy theorem [78]. Thus, asymptotic convergency with the theoretical normal distribution of the variables is assumed.

Table 3. Descriptive statistics of the variables present in the postulated model including prominent FTIR spectral bands of SEM.

Variable	Min	Max	Mean	SE	SD	Variance	Skewness	Kurtosis
[Cu (II)]	0	10	5.43	0.588	3.576	12.787	−0.102	−1.008
[Ag (I)]	0	60	22.43	4.391	26.709	713.363	0.704	−1.480
[Time (days)]	35	49	43.70	0.955	5.811	33.770	−0.495	−1.371
[CHH_DNMT]	0.36	0.76	0.5838	0.02252	0.13698	0.019	−0.194	−1.054
[CHH_SV]	8.48	8.91	8.6546	0.01884	0.11462	0.013	−0.079	−0.754
[1630 . . . 1470]	2.6528	4.6523	3.9617	0.0762	0.4635	0.215	−0.709	0.278
[GPRE]	0.71	6.06	2.5563	0.2727	1.6589	2.752	0.932	−0.122

Pearson’s linear correlation coefficients (Table 4) show that Cu (II) was positively correlated with GPRE, while a negative correlation was evaluated for CHH_SV. Ag(I) was negatively correlated with CHH_DNMV, whereas another culture time was positively correlated with CHH_SV. CHH_DNMV was positively correlated with F1630 ... 1470. The other correlations were insignificant.

Table 4. Pearson’s linear correlation coefficients for analyzed variables.

Variable	[Cu (II)]	[Ag (I)]	[Time (days)]	[CHH_DNMV]	[CHH_SV]	[1630 ... 1470]	[GPRE]
[Cu (II)]	1						
[Ag (I)]	−0.181	1					
[Time (days)]	−0.312	−0.203	1				
[CHH_DNMV]	0.320	−0.426 **	−0.028	1			
[CHH_SV]	−0.386 *	0.050	0.607 **	0.247	1		
[1630 ... 1470]	0.075	−0.020	−0.116	0.389 *	0.080	1	
[GPRE]	0.807 **	−0.201	−0.061	0.005	−0.297	−0.052	1

* Correlation is significant at the 0.05 level (2-tailed); **. Correlation is significant at the 0.01 level (2-tailed).

The model only uses three endogenous variables (CHH_DNMV, CHH_SV, and GPRE) and two observed variables (Cu (II) and F1630...1470). The relationships had a single covariance (Cu(II) and F1630...1470) and were non-recursive. The model included three residuals (Figure 2).

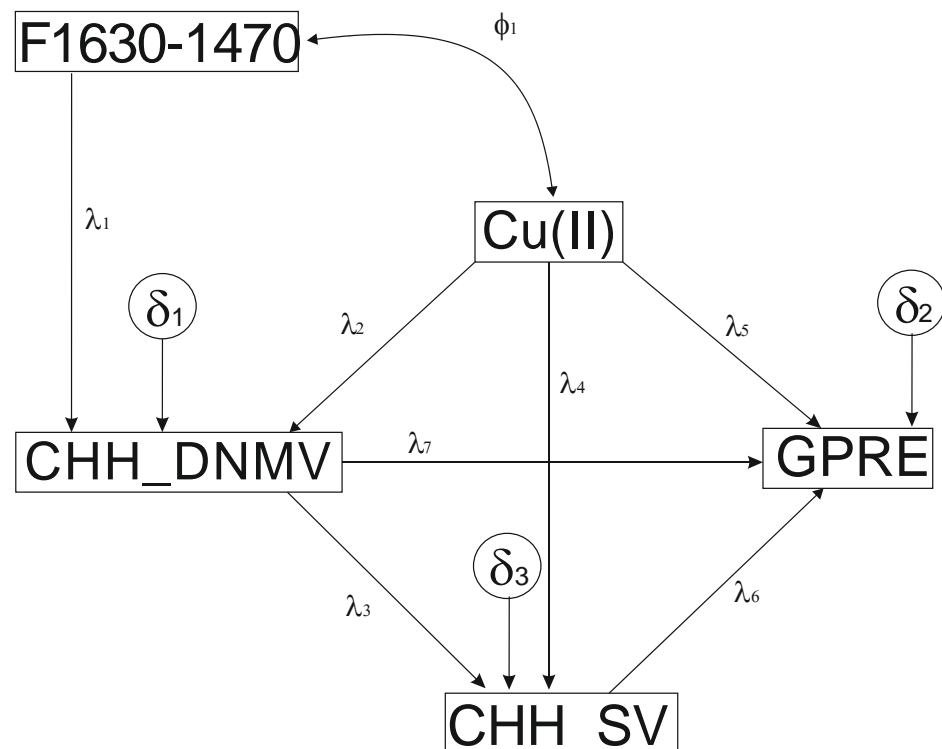


Figure 2. The hypothesized SEM model. Cu(II) ions concentration (μM); GPRE—green plant regeneration efficiency (number of regenerants per 100 plated anthers); the metAFLP quantitative characteristics concerning sequence variation (CHH_SV) and de novo DNA methylation (CHH_DNMV) between donor plant and its regenerants affect asymmetric CHH sequence contexts; The 1630 ... 1470 cm^{-1} wavenumber index represents the FTIR spectrum range assigned to SAM. λ_1 – λ_7 path coefficients, δ_1 – δ_3 residuals (experimental errors), and δ_1 a covariate.

As not all spectra assigned to SAM resulted in significant models, the final model encompassed the combined FTIR F1630_1590 cm^{-1} and F1490_1470 cm^{-1} spectra, resulting in well-fitting models and the most significant paths (Tables 2 and 5). Thus, only the combined model is reported in details.

Table 5. Path coefficients, variances and covariances for the analyzed model.

Parameter	Effect			Estimate (<i>b</i>)	SE	Test Statistic	Standardized (β)
<i>Path coefficients</i>							
λ_1	[1630 ... 1470]	→	[CHH_DNMV]	0.1084	0.0432	2.5118 *	0.3669
λ_2	[Cu(II)]	→	[CHH_DNMV]	0.0112	0.0056	2.0019 **	0.2924
λ_3	[CHH_DNMV]	→	[CHH_SV]	0.3457	0.123	2.8115 **	0.4131
λ_4	[Cu(II)]	→	[CHH_SV]	−0.0166	0.0047	−3.5252 ***	−0.518
λ_5	[Cu(II)]	→	[GPRES]	0.4576	0.0479	9.552 ***	0.9863
λ_6	[CHH_SV]	→	[GPRES]	2.4767	1.4615	1.6947	0.1711
λ_7	[CHH_DNMV]	→	[GPRES]	−4.2763	1.1907	−3.5914 ***	−0.3531
<i>Covariance</i>							
φ_1	Cu(II)	←→	[F1630 ... 1470]	0.1206	0.2695	0.4474	
<i>Variances</i>							
δ_1				0.0139	0.0033	4.24264 ***	
δ_2				0.0089	0.0021	4.24264 ***	
δ_3				0.6859	0.1617	4.24264 ***	
[Cu(II)]				12.4414	2.9325	4.24264 ***	
[1630 ... 1470]				0.209	0.0493	4.24264 ***	

*—significant at $p \leq 0.05$; **—significant at $p \leq 0.01$; ***—significant at $p \leq 0.001$.

An insignificant chi-squared value indicates a well-fitting model when the sample size is large. However, when the sample size is restricted (as in the case of our data), the test may result in incorrect outcomes [79]. In such a case, using the chi-squared test as the information criterion only [80] is suggested. Thus, additional model descriptive goodness-of-fit measures were used for the model fit evaluation. Nearly all the goodness-of-fit measures were close to the cut-off values [81] or exceeded them. The AGFI and GFI were above 0.95 rigorous cut-off value [82]. The PGFI was around 0.13. The PNFI and PCFI were relatively small, indicating model complexity. Still, the SRMR parameter was below 0.05, demonstrating excellent fitting of the hypothesized model to the data. A similar value was evaluated for the RMR. Additionally, TLI and CFI were close to 1, and RMSEA was less than 0.05, which shows that the model fits the experimental data very well (Table 2).

All the paths' (*b*) coefficients of the hypothesized model were significant (Table 5) except for the CHH_SV→GPRES. The effect of Cu(II) on GPRES (β) was the highest and most positive. The effect of Cu(II) on CHH_SV was the next one, but negative, followed by the CHH_DNMV→CHH_SV, which was positive. The impact of the F1630 ... 1470 variable on CHH_DNMV was also significant and positive, whereas CHH_DNMV negatively affected GPRES. The CHH_DNMV→Cu(II) was also positive and the lowest according to absolute values. Cu (II) and F1630-1470 had no significant covariance.

The hypothesized model includes direct, indirect, and total effects (Table 6). The GPRES variable showed the greatest dependence on Cu (II) (direct: $\beta = 0.9863$ and total: $\beta = 0.9863$ with negative indirect: $\beta = -0.1712$ effects). The CHH_SV depended negatively on Cu (II) ($\beta = -0.518$ (direct); $\beta = -0.3972$ (total) and indirect $\beta = 0.1208$ effects)) but positively on CHH_DNMV ($\beta = 0.4131$ direct and total effects). The CHH_DNMV was mostly affected by F1630 ... 1470 via direct and total effects ($\beta = 0.3669$). Finally, the direct effect of Cu (II) ($\beta = 0.2924$) on CHH_DNMV was observed.

Table 6. Direct, indirect and total effects for the analyzed model.

Effect			Estimates (<i>b</i>)			Standardized Estimates (β)		
			Direct	Indirect	Total	Direct	Indirect	Total
[GPRE]								
[1630 ... 1470]	→	[GPRE]	-	-0.3709	-0.3709	-	-0.1036	-0.1036
[Cu(II)]	→	[GPRE]	0.4576	-0.0794	0.3781	0.9863	-0.1712	0.8151
[CHH_DNMV]	→	[GPRE]	-4.2763	0.8562	-3.4201	-0.3531	0.0707	-0.2824
[CHH_SV]	→	[GPRE]	2.4767	-	2.4767	0.1711	-	0.1711
[CHH_SV]								
[1630 ... 1470]	→	[CHH_SV]	-	0.0375	0.0375	-	0.1516	0.1516
[Cu(II)]	→	[CHH_SV]	-0.0166	0.0039	-0.0127	-0.5180	0.1208	-0.3972
[CHH_DNMV]	→	[CHH_SV]	0.3457	-	0.3457	0.4131	-	0.4131
[CHH_DNMV]								
[1630 ... 1470]	→	[CHH_DNMV]	0.1084	-	0.1084	0.3669	-	0.3669
[Cu(II)]	→	[CHH_DNMV]	0.0112	-	0.0112	0.2924	-	0.2924

The model did not account for the time of another culture (T) and the amount of Ag(I). Additionally, any other sequence context (CG or CHG), including SV, DMV, or DNMV, did not work when added to the proposed model.

4. Discussion

Infrared spectroscopy, particularly the FTIR in ATR mode, is a convenient technique widely used for comparative studies of the biochemical profiles of biological materials. It is a fast, label-free, non-destructive, high-throughput approach successfully applied in taxonomic classification, searching for developmental modifications of phenotype, response to growth conditions, and environmental stresses [53,83–87]. It proved its credit in our previous studies on barley leaves [37] from tissue culture to show the involvement of the Yang cycle in response to ionic stress.

Here, we attempted to link the metAFLP quantitative characteristics of tissue culture-induced variation (TCIV), including DNA methylation pattern, sequence variation evaluated in the triticale regenerants, varying times of anther cultures, the S-adenosyl-L-methionine synthesis fluctuations, and GPRE related to variable Cu(II) and Ag(I) ion concentrations in the IM, by employing structural equation modeling to test the hypothesis that all the data could be combined into a single statistical model of GPRE. It is important to note that except for the FTIR data concerning the SAM spectra, all of the other results have already been discussed in our previous papers [46,63]. So, to keep the presentation simple, we focused on the FTIR data and the SEM model.

Generally, the plant leaves showed complex spectra, where bands from multiple compounds, including those from SAM, overlapped in the most informative region between 1700 and 900 cm^{-1} . Thus, identifying a single spectral region characteristic of SAM was hardly possible. We have analyzed the SAM reference compound to identify the most prominent FTIR spectra ranges. We used as the inputs to the model only absorbances for the band regions that corresponded to the most prominent bands of the reference spectrum of SAM. The contribution of each of them was subsequently evaluated by analyzing the model performance. The presented approach was used by us in earlier studies on the input of glutathione in GPRE [81]. However, in those cases, a less complicated banding pattern was observed with just one feature of the GSH spectrum range, which made it easier to choose the right FTIR region.

Out of the five putative regions (Table 2), three of them failed to be informative. The region between 1310 and 1300 cm^{-1} that may be justified by a relatively strong signal from the adenine (the C-C, C=N stretching vibrations, and twisting of CH_2 groups in

methionine) failed to build an SEM model with all informative paths (not shown). As indicated by some goodness-of-fit statistics, the band around 1410 cm^{-1} from the SAM spectrum did not match the model. Overlapping the SAM band vibrations with a strong band centered at 1398 cm^{-1} from multiple tissue compounds could explain the lack of informativeness of the region. Remarkably, this infrared spectrum range may be assigned the O-H in-plane bending mode from phenols and the symmetric stretching of COO- from carboxylic acids. Furthermore, the $1770\text{--}1780\text{ cm}^{-1}$ region related to C=O stretching failed to be helpful in SEM model construction due to the lack of significance of some paths rather than problems with reasonably good goodness-of-fit statistics. Again, we speculated that overlapping signals masked the vibrations from SAM's C=O bands in leaf materials. Lastly, the carbohydrate spectral fingerprint between 1200 and 900 cm^{-1} , which shows the presence of simple sugars and cell wall polysaccharides, was not considered because it was thought to hide weak SAM signals.

On the other hand, the $1470\text{--}1490\text{ cm}^{-1}$ and $1570\text{--}1630\text{ cm}^{-1}$ FTIR spectra ranges allowed the proposed models to have both model-fit indices as expected for excellent model fitting and with significant paths, except for one from SV_CHH to GPRE, which was close to significance ($p = 0.0506$) but turned out to be important in other studies [46]. As the path stabilized the model and was significant in earlier cases [46], we also decided to retain it in the current study. The 1630 to 1590 cm^{-1} range was related to the adenosine and methionine compounds of SAM. Notably, it corresponds to the C-C and C-N stretches in pyrimidine and to the scissoring vibrations of the NH_2 group present in adenine and methionine [72,73,75] band vibrations. This region does not correspond with maximum absorbance leaf spectra and is located on the shoulder of the Amide I band. The amide I band arises from various vibration modes, including C-C, C=O, C=C, C-N stretch, NH_2 scissoring, N-H deformation of amino acids, peptides, and asymmetric stretching of COO- in organic acids and pectins. Its location on the shoulder possibly makes it visible in the model since the region near Amide I peak in the leaf spectra ($1630\text{--}1660\text{ cm}^{-1}$) showed large variability due to the contribution of other more abundant compounds in leaf tissues. Remarkably, the spectral regions outside of this range could interfere with the contributions from amino acids, organic acids, and proteins, the variability of which could mask the effect of SAM. The $1470\text{--}1490\text{ cm}^{-1}$ FTIR spectrum, which reflects C-N, C-C stretching, CH_3 deformation, and NH_2 bending stretching [76], was helpful in the proposed model. As the vibrations were typical for SAM bands (see the FTIR graph of SAM's reference compound), we combined them into a single variable utilized for the model construction. It is worth mentioning that the whole FTIR spectrum range was tested in the model; however, only some regions associated with band vibrations present in SAM resulted in excellent fitting SEM models. So, this proves our theory that FTIR spectra show how SAM affects de novo DNA methylation, thus confirming our hypothesis that FTIR spectra reflect SAM-influencing de novo DNA methylation, which is congruent with the knowledge linking the Yang biochemical cycles.

Despite a limited number of regenerants used to construct the structural equation model, the fit indices confirmed that the model with combined FTIR spectra well fitted the data. Even though some deviation from the variables' normality (indicated by skewness and kurtosis), the deviations were acceptable for further analysis. We have also identified significant correlations between variables, showing that they may be used for model construction. All the paths (maybe except for CHH_SV→GPRES) were significant. As Cu(II) and Ag(I) were used as ingredients added to the IM, the two variables should be treated as exogenous. Usually, it is assumed that such variables impact other variables. However, it could be possible that another non-experimental variables could also act exogenously. On such an occasion, the variable is controlled by an unknown exogenous variable that was not assumed. This is possibly the case in our model where the $F_{1630 \dots 1470\text{ cm}^{-1}}$ variable reflecting some band vibrations from SAM was treated as exogenous. There were no evident relationships between the two exogenous variables (confirmed by the lack of correlation). Furthermore, SAM seems not to influence GPRES. It is possible that

the model needs to be tested with intermediate compounds such as glutathione to show the relationships.

Interestingly, we did not include Ag(I) in the model, which is somewhat surprising given that Ag(I) supplementation in tissue culture media appears to improve plant regeneration efficiency [24,88]. In addition, Orłowska [89] demonstrated the role of Ag(I) in the triticale model. However, the path indicating its influence on GPRE was weak (although significant), as indicated by the standardized β value [89]. It is not surprising that by having a limited number of regenerants and a relatively weak path, only those with substantial effects could be retained in models with some other variables. Thus, the Ag(I) variable was not implemented in the current SEM model. In the same way, the time of anther cultures was not included in the model, even though time affected genetic stability [90] and was included in mediation analyses of the comparable relationship in barley [91]. The insignificance of time of anther culture may indicate that it is less important than the other factors and that a larger sample size is needed to verify its impact on GPRE or TCIV characteristics.

The presented model shows the central role of Cu(II) as it impacts *de novo* DNA methylation and sequence variation of the CHH asymmetric sequence contexts and strongly influences the GPRE. Interestingly, we failed to implement other sequence contexts (CG, CHG) and DNA demethylation in the model. The explanation for that may be linked to the CHH context. It is the least represented methylation type in the cell [92], thus its fluctuations might be easily detected, while the other contexts' changes are averaged. Another possibility is that CHH *de novo* DNA methylation differs slightly from that of CG [93] and CHG [94,95]. Chromomethylase 2 (CMT2) [96] and DOMAINS REARRANGED METHYLTRANSFERASE 1/2 (DRM1/2) must establish *de novo* methylation in the CHH sequence in each generation via the RNA-directed DNA methylation (RdDM) pathway [97]. Whatever the reason, our model demonstrates that SAM influences the CHH sequence context. This is clearly in agreement with the role of SAM in the cell, at least in the case of that sequence context.

Our model is congruent with the putative oxidative stress mechanism that may lead to mutations via the modification of methylated cytosines [98,99] and demonstrates that *de novo* DNA methylation may participate in GPRE. However, Cu(II) is the most critical factor impacting GPRE. Given the roles of CHH_DNMV and that Cu(II) acts as a cofactor in many biochemical pathways, this could affect the epigenetics that allow GPRE to function. In this context, the role of glutathione should be tested. If the compound changes GPRE, this would be strong evidence that epigenetics plays a role in GPRE.

Surprisingly, SV within the CHH context did not influence GPRE. Sequence variation is one of the causes of somaclonal variation, according to the data [100–103]. The discrepancy could be explained by the tiny abundance of the CHH methylated sequence in the genome compared to the symmetric contexts. If so, then, as could be expected, our model failed to detect minor effects. Alternatively, a limited sample size might have influenced the statistics, limiting the results. In this context, the presented model should be treated cautiously, demonstrating a putative way of analyzing complex phenomena affecting *in vitro* tissue culture plant regeneration. However, the model makes it clear that changing the components of the medium can improve GPRE and explains why it is important to understand GPRE in triticale.

5. Conclusions

Our results showed that combining metaAFLP, biochemical, and absorbance data from infrared spectroscopy evaluated on regenerants derived using a specially designed tissue culture model, limiting pre-existing variation and statistical approaches such as SEM, makes it possible to construct a theory-based model reflecting biological phenomena related to GPRE and demonstrating relationships between variables. We have demonstrated that Cu(II) ions in the IM are the critical factors affecting GPRE. By manipulating their concentrations, it is possible to change the balance of green plant regeneration efficiency. Furthermore, we have shown that SAM is also involved in GPRE indirectly via methyla-

tion of the CHH asymmetric sequence contexts via de novo methylation, indicating the involvement of the Yang cycle in GPRE. Our model may miss a significant variable that we did not assume. The putative candidate factor may be glutathione due to its positive effect on microspore embryogenesis in rye [104], the number of embryo-like structures in triticale [105], or embryogenic development in Arabidopsis [106]. Finally, all of these features may influence green plant regeneration efficiency.

Author Contributions: Conceptualization, R.O. and P.T.B.; methodology, R.O. and P.T.B.; formal analysis, R.O., J.Z. (Janusz Zimny), J.Z. (Jacek Zebrowski); investigation, R.O., J.Z. (Janusz Zimny) and P.A.; writing—original draft preparation, P.T.B., R.O., J.Z. (Janusz Zimny), J.Z. (Jacek Zebrowski) and P.A.; writing—review and editing, R.O.; visualization, P.T.B., R.O., J.Z. (Jacek Zebrowski) and P.A.; supervision, R.O.; project administration, P.T.B. and R.O.; funding acquisition, P.T.B. All authors have read and agreed to the published version of the manuscript.

Funding: This research was funded by ministry of agriculture and rural development, Poland, grant number HORhn-801-PB-22/15-18.

Institutional Review Board Statement: Not applicable.

Informed Consent Statement: Not applicable.

Data Availability Statement: Not applicable.

Acknowledgments: Not applicable.

Conflicts of Interest: The authors declare no conflict of interest. The funders had no role in the design of the study; in the collection, analyses, or interpretation of data; in the writing of the manuscript; or in the decision to publish the results.

References

- Sapra, V.T.; Heyne, E.G.; Wilkins, H.D. Triticale, a Man-Made Species of a Crop Plant. *Trans. Kans. Acad. Sci.* **1971**, *74*, 52. [\[CrossRef\]](#)
- Eudes, F.; Chugh, A. An Overview of Triticale Doubled Haploids. In *Advances in Haploid Production in Higher Plants*; Touraev, A., Forster, B.P., Jain, S.M., Eds.; Springer: Dordrecht, The Netherlands, 2009; pp. 87–96.
- The Role of Polyploidization and Interspecific Hybridization in the Breeding of Ornamental Crops. In *Polyploidy and Hybridization for Crop Improvement*; CRC Press: Boca Raton, FL, USA, 2017; pp. 175–197. [\[CrossRef\]](#)
- Wędzony, M. Protocol for anther culture in hexaploid triticale (\times *Triticosecale* Wittm.). In *Doubled Haploid Production in Crop Plants: A manual*; Maluszynski, M., Kasha, K.J., Forster, B.P., Szarejko, I., Eds.; Kluwer Academic Publishers: Dordrecht, The Netherlands; Boston, MA, USA; London, UK, 2003; pp. 135–140.
- Lantos, C.; Bóna, L.; Boda, K.; Pauk, J. Comparative analysis of in vitro anther- and isolated microspore culture in hexaploid Triticale (\times *Triticosecale* Wittmack) for androgenic parameters. *Euphytica* **2013**, *197*, 27–37. [\[CrossRef\]](#)
- Oleszczuk, S.; Sowa, S.; Zimny, J. Direct embryogenesis and green plant regeneration from isolated microspores of hexaploid triticale (\times *Triticosecale* Wittmack) cv. Bogo. *Plant Cell Rep.* **2004**, *22*, 885–893. [\[CrossRef\]](#)
- Machczyńska, J.; Orłowska, R.; Mańkowski, D.R.; Zimny, J.; Bednarek, P.T. DNA methylation changes in triticale due to in vitro culture plant regeneration and consecutive reproduction. *Plant Cell Tissue Organ Cult. (PCTOC)* **2014**, *119*, 289–299. [\[CrossRef\]](#)
- Ponitka, A.; Slusarkiewicz-Jarzina, A.; Wędzony, M.; Marcinska, I.; Wozna, J. The influence of various in vitro culture conditions on androgenetic embryo induction and plant regeneration from hexaploid triticale [\times *Triticosecale* Wittm.]. *J. Appl. Genet.* **1999**, *40*, 165–174.
- Muranty, H.; Sourdille, P.; Bernard, S.; Bernard, M. Genetic characterization of spontaneous diploid androgenetic wheat and triticale plants. *Plant Breed.* **2002**, *121*, 470–474. [\[CrossRef\]](#)
- Ślusarkiewicz-Jarzina, A.; Pudelska, H.; Woźna, J.; Pniewski, T. Improved production of doubled haploids of winter and spring triticale hybrids via combination of colchicine treatments on anthers and regenerated plants. *J. Appl. Genet.* **2017**, *58*, 287–295. [\[CrossRef\]](#)
- Gonzalez, M.; Hernández, I.; Jouve, N. Analysis of anther culture response in hexaploid triticale. *Plant Breed.* **1997**, *116*, 302–304. [\[CrossRef\]](#)
- Krzewska, M.; Czyczyło-Mysza, I.; Dubas, E.; Golebiowska, G.; Żur, I. Identification of QTLs associated with albino plant formation and some new facts concerning green versus albino ratio determinants in triticale (\times *Triticosecale* Wittm.) anther culture. *Euphytica* **2015**, *206*, 263–278. [\[CrossRef\]](#)
- Pauk, J.; Puolimatka, M.; Tóth, K.L.; Monostori, T. In vitro androgenesis of triticale in isolated microspore culture. *Plant Cell Tissue Organ Cult. (PCTOC)* **2000**, *61*, 221–229. [\[CrossRef\]](#)
- Makowska, K.; Oleszczuk, S. Albinism in barley androgenesis. *Plant Cell Rep.* **2013**, *33*, 385–392. [\[CrossRef\]](#) [\[PubMed\]](#)

15. Gajecka, M.; Marzec, M.; Chmielewska, B.; Jelonek, J.; Zbieszczak, J.; Szarejko, I. Changes in plastid biogenesis leading to the formation of albino regenerants in barley microspore culture. *BMC Plant Biol.* **2021**, *21*, 1–24. [[CrossRef](#)] [[PubMed](#)]
16. Sakamoto, W.; Miyagishima, S.-y.; Jarvis, P. Chloroplast Biogenesis: Control of Plastid Development, Protein Import, Division and Inheritance. *Arab. Book* **2008**, *6*, e0110. [[CrossRef](#)] [[PubMed](#)]
17. Clément, C.; Pacini, E. Anther plastids in angiosperms. *Bot. Rev.* **2001**, *67*, 54–73. [[CrossRef](#)]
18. Ruppel, N.J.; Logsdon, C.A.; Whippo, C.W.; Inoue, K.; Hangarter, R.P. A mutation in Arabidopsis SEEDLING PLASTID DEVELOPMENT1 affects plastid differentiation in embryo-derived tissues during seedling growth. *Plant Physiol.* **2011**, *155*, 342–353. [[CrossRef](#)] [[PubMed](#)]
19. Steiner, S.; Schröter, Y.; Pfalz, J.; Pfannschmidt, T. Identification of Essential Subunits in the Plastid-Encoded RNA Polymerase Complex Reveals Building Blocks for Proper Plastid Development. *Plant Physiol.* **2011**, *157*, 1043–1055. [[CrossRef](#)]
20. García-Alcázar, M.; Giménez, E.; Pineda, B.; Capel, C.; García-Sogo, B.; Sánchez, S.; Yuste-Lisbona, F.J.; Angosto, T.; Capel, J.; Moreno, V.; et al. Albino T-DNA tomato mutant reveals a key function of 1-deoxy-D-xylulose-5-phosphate synthase (DXS1) in plant development and survival. *Sci. Rep.* **2017**, *7*, 45333. [[CrossRef](#)]
21. Immonen, S.; Robinson, J. Stress treatments and ficoll for improving green plant regeneration in triticales anther culture. *Plant Sci.* **2000**, *150*, 77–84. [[CrossRef](#)]
22. Nirwan, R.S.; Kothari, S.L. High copper levels improve callus induction and plant regeneration in *Sorghum bicolor* (L.) Moench. *Vitr. Cell. Dev. Biol.-Plant* **2003**, *39*, 161–164. [[CrossRef](#)]
23. Echavarrí, B.; Soriano, M.; Cistué, L.; Valles, M.P.; Castillo, A.M. Zinc sulphate improved microspore embryogenesis in barley. *Plant Cell Tissue Organ Cult. (PCTOC)* **2008**, *93*, 295–301. [[CrossRef](#)]
24. Hassan, M.F.; Islam, S. Effect of silver nitrate and growth regulators to enhance anther culture response in wheat (*Triticum aestivum* L.). *Heliyon* **2021**, *7*, e07075. [[CrossRef](#)] [[PubMed](#)]
25. Orłowska, R.; Pachota, K.A.; Machczyńska, J.; Niedziela, A.; Makowska, K.; Zimny, J.; Bednarek, P.T. Improvement of anther cultures conditions using the Taguchi method in three cereal crops. *Electron. J. Biotechnol.* **2019**, *43*, 8–15. [[CrossRef](#)]
26. Eaguirre, G.; Epsilon, M. Copper Delivery to Chloroplast Proteins and its Regulation. *Front. Plant Sci.* **2016**, *6*, 1250. [[CrossRef](#)] [[PubMed](#)]
27. Horn, D.; Barrientos, A. Mitochondrial copper metabolism and delivery to cytochrome oxidase. *IUBMB Life* **2008**, *60*, 421–429. [[CrossRef](#)]
28. Cohu, C.M.; Pilon, M. Regulation of superoxide dismutase expression by copper availability. *Physiol. Plant.* **2007**, *129*, 747–755. [[CrossRef](#)]
29. Henriques, F.S. Effects of Copper Deficiency on the Photosynthetic Apparatus of Sugar beet (*Beta vulgaris* L.). *J. Plant Physiol.* **1989**, *135*, 453–458. [[CrossRef](#)]
30. Abdel-Ghany, S.E.; Pilon, M. MicroRNA-mediated Systemic Down-regulation of Copper Protein Expression in Response to Low Copper Availability in Arabidopsis. *J. Biol. Chem.* **2008**, *283*, 15932–15945. [[CrossRef](#)]
31. Maksymiec, W. Effect of copper on cellular processes in higher plants. *Photosynthetica* **1997**, *34*, 321–342. [[CrossRef](#)]
32. Dahan, J.; Tcherkez, G.; Macherel, D.; Benamar, A.; Belcram, K.; Quadrado, M.; Arnal, N.; Mireau, H. Disruption of the CYTOCHROME C OXIDASE DEFICIENT1 Gene Leads to Cytochrome c Oxidase Depletion and Reorchestrated Respiratory Metabolism in Arabidopsis. *Plant Physiol.* **2014**, *166*, 1788–1802. [[CrossRef](#)]
33. Ji, J.; Huang, W.; Yin, C.; Gong, Z. Mitochondrial Cytochrome c Oxidase and F1Fo-ATPase Dysfunction in Peppers (*Capsicum annuum* L.) with Cyttoplasmic Male Sterility and Its Association with orf507 and Ψatp6-2 Genes. *Int. J. Mol. Sci.* **2013**, *14*, 1050–1068. [[CrossRef](#)]
34. Bligny, R.; Douce, R. Mitochondria of Isolated Plant Cells (*Acer pseudoplatanus* L.): II. Copper Deficiency Effects on Cytochrome C Oxidase and Oxygen Uptake. *Plant Physiol.* **1977**, *60*, 675–679. [[CrossRef](#)]
35. Van de Poel, B.; Bulens, I.; Markoula, A.; Hertog, M.; Dreesen, R.; Wirtz, M.; Vandoninck, S.; Oppermann, Y.; Keulemans, J.; Hell, R.; et al. Targeted Systems Biology Profiling of Tomato Fruit Reveals Coordination of the Yang Cycle and a Distinct Regulation of Ethylene Biosynthesis during Postclimacteric Ripening. *Plant Physiol.* **2012**, *160*, 1498–1514. [[CrossRef](#)]
36. Watanabe, M.; Chiba, Y.; Hirai, M.Y. Metabolism and Regulatory Functions of O-Acetylserine, S-Adenosylmethionine, Homocysteine, and Serine in Plant Development and Environmental Responses. *Front. Plant Sci.* **2021**, *12*. [[CrossRef](#)] [[PubMed](#)]
37. Bednarek, P.T.; Zebrowski, J.; Orłowska, R. Exploring the Biochemical Origin of DNA Sequence Variation in Barley Plants Regenerated via in Vitro Anther Culture. *Int. J. Mol. Sci.* **2020**, *21*, 5770. [[CrossRef](#)] [[PubMed](#)]
38. Li, W.; Han, Y.; Tao, F.; Chong, K. Knockdown of SAMS genes encoding S-adenosyl-L-methionine synthetases causes methylation alterations of DNAs and histones and leads to late flowering in rice. *J. Plant Physiol.* **2011**, *168*, 1837–1843. [[CrossRef](#)] [[PubMed](#)]
39. Chiba, Y.; Sakurai, R.; Yoshino, M.; Ominato, K.; Ishikawa, M.; Onouchi, H.; Naito, S. S-adenosyl-L-methionine is an effector in the posttranscriptional autoregulation of the cystathionine γ -synthase gene in Arabidopsis. *Proc. Natl. Acad. Sci. USA* **2003**, *100*, 10225–10230. [[CrossRef](#)]
40. Larkin, P.J.; Scowcroft, W.R. Somaclonal variation — A novel source of variability from cell cultures for plant improvement. *Theor. Appl. Genet.* **1981**, *60*, 197–214. [[CrossRef](#)]
41. Evans, D.; Sharp, W.R.; Medina-Filho, H.P. Somaclonal and gametoclonal variation. *Am. J. Bot.* **1984**, *71*, 759–774. [[CrossRef](#)]
42. Bednarek, P.T.; Orłowska, R.; Koebner, R.M.D.; Zimny, J. Quantification of the tissue-culture induced variation in barley (*Hordeum vulgare* L.). *BMC Plant Biol.* **2007**, *7*, 10. [[CrossRef](#)]

43. Bednarek, P.T.; Orłowska, R. Time of In Vitro Anther Culture May Moderate Action of Copper and Silver Ions that Affect the Relationship between DNA Methylation Change and the Yield of Barley Green Regenerants. *Plants* **2020**, *9*, 1064. [CrossRef]
44. Bednarek, P.T.; Orłowska, R.; Mańkowski, D.R.; Oleszczuk, S.; Zebrowski, J. Structural Equation Modeling (SEM) Analysis of Sequence Variation and Green Plant Regeneration via Anther Culture in Barley. *Cells* **2021**, *10*, 2774. [CrossRef] [PubMed]
45. Orłowska, R.; Bednarek, P.T. Precise evaluation of tissue culture-induced variation during optimisation of in vitro regeneration regime in barley. *Plant Mol. Biol.* **2020**, *103*, 33–50. [CrossRef] [PubMed]
46. Orłowska, R.; Pachota, K.A.; Androsiuk, P.; Bednarek, P.T. Triticale Green Plant Regeneration Is Due to DNA Methylation and Sequence Changes Affecting Distinct Sequence Contexts in the Presence of Copper Ions in Induction Medium. *Cells* **2021**, *11*, 84. [CrossRef] [PubMed]
47. Lahlali, R.; Jiang, Y.; Kumar, S.; Karunakaran, C.; Liu, X.; Borondics, F.; Hallin, E.; Bueckert, R. ATR-FTIR spectroscopy reveals involvement of lipids and proteins of intact pea pollen grains to heat stress tolerance. *Front. Plant Sci.* **2014**, *5*. [CrossRef]
48. Alonso-Simón, A.; García-Angulo, P.; Mérida, H.; Encina, A.; Álvarez, J.M.; Acebes, J.L. The use of FTIR spectroscopy to monitor modifications in plant cell wall architecture caused by cellulose biosynthesis inhibitors. *Plant Signal. Behav.* **2011**, *6*, 1104–1110. [CrossRef]
49. Skolik, P.; McAinsh, M.R.; Martin, F.L. ATR-FTIR spectroscopy non-destructively detects damage-induced sour rot infection in whole tomato fruit. *Planta* **2018**, *249*, 925–939. [CrossRef]
50. Sharma, S.; Uttam, K.N. Early Diagnosis of Mercury Stress of Wheat Seedlings Using Attenuated Total Reflection Fourier Transform Infrared Spectroscopy. *Anal. Lett.* **2018**, *51*, 1544–1563. [CrossRef]
51. Acemi, A. Monitoring the effects of chitosan on the profile of certain cell wall and membrane biomolecules in the leaves of *Eruca vesicaria* ssp. sativa through FT-IR spectroscopy. *Plant Physiol. Biochem.* **2022**, *173*, 25–32. [CrossRef]
52. Osman, S.O.M.; Saad, A.S.I.; Tadano, S.; Takeda, Y.; Konaka, T.; Yamasaki, Y.; Tahir, I.S.A.; Tsujimoto, H.; Akashi, K. Chemical Fingerprinting of Heat Stress Responses in the Leaves of Common Wheat by Fourier Transform Infrared Spectroscopy. *Int. J. Mol. Sci.* **2022**, *23*, 2842. [CrossRef]
53. Bağcıoğlu, M.; Kohler, A.; Seifert, S.; Kneipp, J.; Zimmermann, B. Monitoring of plant–environment interactions by high-throughput FTIR spectroscopy of pollen. *Methods Ecol. Evol.* **2016**, *8*, 870–880. [CrossRef]
54. Wang, J.; Zhu, J.; Huang, R.; Yang, Y. Investigation of cell wall composition related to stem lodging resistance in wheat (*Triticum aestivum* L.) by FTIR spectroscopy. *Plant Signal. Behav.* **2012**, *7*, 856–863. [CrossRef] [PubMed]
55. Meinen, C.; Rauber, R. Root discrimination of closely related crop and weed species using FT MIR-ATR spectroscopy. *Front. Plant Sci.* **2015**, *6*. [CrossRef] [PubMed]
56. Buitrago, M.F.; Skidmore, A.K.; Groen, T.A.; Hecker, C.A. Connecting infrared spectra with plant traits to identify species. *ISPRS J. Photogramm. Remote Sens.* **2018**, *139*, 183–200. [CrossRef]
57. Holden, C.A.; Bailey, J.P.; Taylor, J.E.; Martin, F.; Beckett, P.; McAinsh, M. Know your enemy: Application of ATR-FTIR spectroscopy to invasive species control. *PLoS ONE* **2022**, *17*, e0261742. [CrossRef] [PubMed]
58. Pour, A.S.; Chegini, G.; Massah, J. Classification of Anthurium flower cultivars based on combination of PCA, LDA and SVM classifier. *CIGR J.* **2018**, *20*, 219–228.
59. Rana, R.; Herz, K.; Bruelheide, H.; Dietz, S.; Haider, S.; Jandt, U.; Pena, R. Leaf Attenuated Total Reflection Fourier Transform Infrared (ATR-FTIR) biochemical profile of grassland plant species related to land-use intensity. *Ecol. Indic.* **2018**, *84*, 803–810. [CrossRef]
60. Johnson, J.; Mani, J.; Ashwath, N.; Naiker, M. Potential for Fourier transform infrared (FTIR) spectroscopy toward predicting antioxidant and phenolic contents in powdered plant matrices. *Spectrochim. Acta Part A Mol. Biomol. Spectrosc.* **2020**, *233*, 118228. [CrossRef]
61. Mann, D.; Labbé, N.; Sykes, R.W.; Gracom, K.; Kline, L.; Swamidoss, I.M.; Burriss, J.N.; Davis, M.; Stewart, N. Rapid Assessment of Lignin Content and Structure in Switchgrass (*Panicum virgatum* L.) Grown Under Different Environmental Conditions. *BioEnergy Res.* **2009**, *2*, 246–256. [CrossRef]
62. Aouidi, F.; Dupuy, N.; Artaud, J.; Roussos, S.; Msallem, M.; Gaime, I.P.; Hamdi, M. Rapid quantitative determination of oleuropein in olive leaves (*Olea europaea*) using mid-infrared spectroscopy combined with chemometric analyses. *Ind. Crop. Prod.* **2012**, *37*, 292–297. [CrossRef]
63. Pachota, K.A.; Orłowska, R.; Bednarek, P.T. Medium composition affects the tissue culture-induced variation in triticale regenerants. *Plant Cell Tissue Organ Cult. (PCTOC)* **2022**, 1–12. [CrossRef]
64. Machczyńska, J.; Orłowska, R.; Zimny, J.; Bednarek, P.T. Extended metAFLP approach in studies of tissue culture induced variation (TCIV) in triticale. *Mol. Breed.* **2014**, *34*, 845–854. [CrossRef] [PubMed]
65. Hanson, B.A. *ChemoSpec: Exploratory Chemometrics for Spectroscopy*, R Package Version 4.4; DePauw University: Greencastle, IN, USA. 2017. Available online: <https://CRAN.R-project.org/package=ChemoSpec> (accessed on 12 December 2017).
66. R Core Team. *R: A Language and Environment for Statistical Computing*; R Foundation for Statistical Computing: Vienna, Austria, 2012; Available online: <https://www.R-project.org/> (accessed on 19 April 2022).
67. Arbuckle, J.L. *Amos*, Version 27.0; IBM SPSS: Chicago, IL, USA. 2014.
68. *IBM Corp IBM SPSS Statistics for Windows*, Version 28.0.0; IBM Corp: Armonk, NY, USA. 2021.
69. Levenberg, K. A method for the solution of certain non-linear problems in least squares. *Q. Appl. Math.* **1944**, *2*, 164–168. [CrossRef]

70. Madsen, K.; Nielsen, H.B.; Tingleff, O. Methods for non-linear least squares problems. In *Informatics and Mathematical Modeling*; Technical University of Denmark: Kongens Lyngby, Denmark, 2004.
71. Marquardt, D.W. An Algorithm for Least-Squares Estimation of Nonlinear Parameters. *J. Soc. Ind. Appl. Math.* **1963**, *11*, 431–441. [[CrossRef](#)]
72. Bergo, V.; Mamaev, S.; Olejnik, J.; Rothschild, K.J. Methionine Changes in Bacteriorhodopsin Detected by FTIR and Cell-Free Selenomethionine Substitution. *Biophys. J.* **2003**, *84*, 960–966. [[CrossRef](#)]
73. Cao, X.; Fischer, G. Conformational and Infrared Spectral Studies of L-Methionine and Its N-Deuterated Isotopomer as Isolated Zwitterions. *J. Phys. Chem. A* **2001**, *106*, 41–50. [[CrossRef](#)]
74. Toyama, A.; Hanada, N.; Abe, Y.; Takeuchi, H.; Harada, I. Assignment of adenine ring in-plane vibrations in adenosine on the basis of ¹⁵N and ¹³C isotopic frequency shifts and TUV resonance Raman enhancement. *J. Raman Spectrosc.* **1994**, *25*, 623–630. [[CrossRef](#)]
75. Bakkiyaraj, D.; Periandy, S.; Xavier, S. Molecular structural investigation of adenosine using spectroscopic and quantum computational calculations. *J. Mol. Struct.* **2016**, *1119*, 490–504. [[CrossRef](#)]
76. Sjöberg, B.; Foley, S.; Cardey, B.; Enescu, M. An experimental and theoretical study of the amino acid side chain Raman bands in proteins. *Spectrochim. Acta Part A Mol. Biomol. Spectrosc.* **2014**, *128*, 300–311. [[CrossRef](#)]
77. Wiercigroch, E.; Szafraniec, E.; Czamara, K.; Pacia, M.Z.; Majzner, K.; Kochan, K.; Kaczor, A.; Baranska, M.; Malek, K. Raman and infrared spectroscopy of carbohydrates: A review. *Spectrochim. Acta Part A Mol. Biomol. Spectrosc.* **2017**, *185*, 317–335. [[CrossRef](#)]
78. Taboga, M. *Lectures on Probability Theory and Mathematical Statistics*; CreateSpace Independent Publishing Platform: North Charleston, SC, USA, 2012.
79. Kenny, D.A.; McCoach, D.B. Effect of the Number of Variables on Measures of Fit in Structural Equation Modeling. *Struct. Equ. Model. Multidiscip. J.* **2003**, *10*, 333–351. [[CrossRef](#)]
80. MacCallum, R.C.; Browne, M.W.; Sugawara, H.M. Power analysis and determination of sample size for covariance structure modeling. *Psychol. Methods* **1996**, *1*, 130–149. [[CrossRef](#)]
81. Bednarek, P.T.; Orłowska, R.; Mańkowski, D.R.; Zimny, J.; Kowalczyk, K.; Nowak, M.; Zebrowski, J. Glutathione and copper ions as critical factors of green plant regeneration efficiency of triticale in vitro anther culture. *Front. Plant Sci.* **2022**, *13*. [[CrossRef](#)] [[PubMed](#)]
82. Mulaik, S.A.; James, L.R.; Van Alstine, J.; Bennett, N.; Lind, S.; Stilwell, C.D. Evaluation of goodness-of-fit indices for structural equation models. *Psychol. Bull.* **1989**, *105*, 430–445. [[CrossRef](#)]
83. Holden, C.A.; Morais, C.L.M.; Taylor, J.E.; Martin, F.L.; Beckett, P.; McAinsh, M. Regional differences in clonal Japanese knotweed revealed by chemometrics-linked attenuated total reflection Fourier-transform infrared spectroscopy. *BMC Plant Biol.* **2021**, *21*, 1–20. [[CrossRef](#)]
84. Kim, S.W.; Ban, S.H.; Chung, H.J.; Cho, S.; Choi, P.S.; Yoo, O.J.; Liu, J.R. Taxonomic discrimination of flowering plants by multivariate analysis of Fourier transform infrared spectroscopy data. *Plant Cell Rep.* **2004**, *23*, 246–250. [[CrossRef](#)]
85. Demir, P.; Onde, S.; Severcan, F. Phylogeny of cultivated and wild wheat species using ATR-FTIR spectroscopy. *Spectrochim. Acta Part A Mol. Biomol. Spectrosc.* **2015**, *135*, 757–763. [[CrossRef](#)]
86. Sharma, S.; Uttam, K.N. Early Stage Detection of Stress Due to Copper on Maize (*Zea mays* L.) by Laser-Induced Fluorescence and Infrared Spectroscopy. *J. Appl. Spectrosc.* **2018**, *85*, 771–780. [[CrossRef](#)]
87. Podgórska, A.; Burian, M.; Gieczewska, K.; Ostaszewska-Bugajska, M.; Zebrowski, J.; Solecka, D.; Szal, B. Altered Cell Wall Plasticity Can Restrict Plant Growth under Ammonium Nutrition. *Front. Plant Sci.* **2017**, *8*, 1344. [[CrossRef](#)]
88. Morshed, S.; Siddique, A.B.; Islam, S.S. Effect of silver nitrate and carbon sources on callus induction and regeneration in maize (*Zea mays* L.). *Appl. Biol. Res.* **2016**, *18*, 252. [[CrossRef](#)]
89. Orłowska, R. Relationships between de novo methylation and green regeneration efficiency in triticale based on structural equation modeling. *J. Appl. Genet.* **2022**. [[CrossRef](#)]
90. Marum, L.; Rocheta, M.; Maroco, J.; Oliveira, M.M.; Miguel, C. Analysis of genetic stability at SSR loci during somatic embryogenesis in maritime pine (*Pinus pinaster*). *Plant Cell Rep.* **2009**, *28*, 673–682. [[CrossRef](#)] [[PubMed](#)]
91. Bednarek, P.T.; Orłowska, R. CG Demethylation Leads to Sequence Mutations in an Anther Culture of Barley Due to the Presence of Cu, Ag Ions in the Medium and Culture Time. *Int. J. Mol. Sci.* **2020**, *21*, 4401. [[CrossRef](#)] [[PubMed](#)]
92. Ni, P.; Huang, N.; Nie, F.; Zhang, J.; Zhang, Z.; Wu, B.; Bai, L.; Liu, W.; Xiao, C.-L.; Luo, F.; et al. Genome-wide Detection of Cytosine Methylations in Plant from Nanopore sequencing data using Deep Learning. *Nat. Commun.* **2021**, *12*, 5976. [[CrossRef](#)]
93. Law, J.A.; Jacobsen, S.E. Establishing, maintaining and modifying DNA methylation patterns in plants and animals. *Nat. Rev. Genet.* **2010**, *11*, 204–220. [[CrossRef](#)] [[PubMed](#)]
94. Bartee, L.; Malagnac, F.; Bender, J. *Arabidopsis cmt3* chromomethylase mutations block non-CG methylation and silencing of an endogenous gene. *Genes Dev.* **2001**, *15*, 1753–1758. [[CrossRef](#)]
95. Lindroth, A.M.; Cao, X.; Jackson, J.P.; Zilberman, D.; McCallum, C.M.; Henikoff, S.; Jacobsen, S.E. Requirement of *CHROMOMETHYLASE3* for Maintenance of CpXpG Methylation. *Science* **2001**, *292*, 2077–2080. [[CrossRef](#)]
96. Stroud, H.; Do, T.; Du, J.; Zhong, X.; Feng, S.; Johnson, L.; Patel, D.J.; Jacobsen, S.E. Non-CG methylation patterns shape the epigenetic landscape in *Arabidopsis*. *Nat. Struct. Mol. Biol.* **2014**, *21*, 64–72. [[CrossRef](#)]
97. Matzke, M.A.; Mosher, R.A. RNA-directed DNA methylation: An epigenetic pathway of increasing complexity. *Nat. Rev. Genet.* **2014**, *15*, 394–408. [[CrossRef](#)]

98. Kreutzer, D.A.; Essigmann, J.M. Oxidized, deaminated cytosines are a source of C → T transitions in vivo. *Proc. Natl. Acad. Sci. USA* **1998**, *95*, 3578–3582. [[CrossRef](#)]
99. Tang, Y.; Xiong, J.; Jiang, H.-P.; Zheng, S.-J.; Feng, Y.-Q.; Yuan, B.-F. Determination of Oxidation Products of 5-Methylcytosine in Plants by Chemical Derivatization Coupled with Liquid Chromatography/Tandem Mass Spectrometry Analysis. *Anal. Chem.* **2014**, *86*, 7764–7772. [[CrossRef](#)]
100. Machczyńska, J.; Zimny, J.; Bednarek, P.T. Tissue culture-induced genetic and epigenetic variation in triticale (\times *Triticosecale* spp. Wittmack ex A. Camus 1927) regenerants. *Plant Mol. Biol.* **2015**, *89*, 279–292. [[CrossRef](#)] [[PubMed](#)]
101. Kacem, N.S.; Muhovski, Y.; Djekoun, A.; Watillon, B. Molecular characterization of genetic variation in somaclones of durum wheat (*Triticum durum* Desf) using SSR markers. *Eur. Sci. J. ESJ* **2017**, *13*. [[CrossRef](#)]
102. Fiuk, A.; Bednarek, P.T.; Rybczyński, J.J. Flow Cytometry, HPLC-RP, and metAFLP Analyses to Assess Genetic Variability in Somatic Embryo-Derived Plantlets of *Gentiana pannonica* Scop. *Plant Mol. Biol. Rep.* **2010**, *28*, 413–420. [[CrossRef](#)]
103. Orłowska, R.; Pachota, K.; Dynkowska, W.; Niedziela, A.; Bednarek, P. Androgenic-Induced Transposable Elements Dependent Sequence Variation in Barley. *Int. J. Mol. Sci.* **2021**, *22*, 6783. [[CrossRef](#)]
104. Zieliński, K.; Krzewska, M.; Żur, I.; Juzoń, K.; Kopeć, P.; Nowicka, A.; Moravčíková, J.; Skrzypek, E.; Dubas, E. The effect of glutathione and mannitol on androgenesis in anther and isolated microspore cultures of rye (*Secale cereale* L.). *Plant Cell Tissue Organ Cult. (PCTOC)* **2020**, *140*, 577–592. [[CrossRef](#)]
105. Żur, I.; Dubas, E.; Krzewska, M.; Zieliński, K.; Fodor, J.; Janowiak, F. Glutathione provides antioxidative defence and promotes microspore-derived embryo development in isolated microspore cultures of triticale (\times *Triticosecale* Wittm.). *Plant Cell Rep.* **2018**, *38*, 195–209. [[CrossRef](#)]
106. Kudelko, K.; Gaj, M.D. Glutathione (GSH) induces embryogenic response in in vitro cultured explants of *Arabidopsis thaliana* via auxin-related mechanism. *Plant Growth Regul.* **2019**, *89*, 25–36. [[CrossRef](#)]